DETECTING GLASS ON THE KRAFLA LAVA FLOW FIELD, ICELAND F. B. Wróblewski[1] and E. L. Rader[1], [1]Department of Earth and Spatial Sciences, University of Idaho, 875 Perimeter Drive MS 3021, Moscow, ID (frankw@uidaho.edu)

Introduction: Where did water once exist, and how much was there? The changing structure of lava flow surfaces has long been a suggested proxy for the available budget of water on Earth and Mars [1]. Depending on the ratio of lava and water, flows will produce features like rootless cones, pillow lavas, and volcanic glass [2], yet, the distribution of glass itself on lava flow surfaces has only been recently investigated [3]. Glass, formed by rapidly cooling volcanic material, is a material that lacks crystalline structure [4]. Thus, detecting glass spectrally is problematic with conventional methods in the visible and near-infrared (VNIR) range as the material lacks diagnostic spectral features due to the diffusion of light. Even when spectral features are present, glass is difficult to distinguish from olivine or other nesosilicates [5]. Instead, detecting glass with VNIR spectra may be more successful by considering the material's lower total (average) reflectance to crystalline or organic materials [6].

On Earth and Mars, the proportion of glass on lava flow surfaces may be categorized into facies of temperature and density between the lava and quenching agent, such as from air, water, or ice. This is important for lava flows because if glass content changes across a flow surface, this may show the environmental conditions into which a lava flow was emplaced, complementary to studying flow morphology. Thus, to begin searching for glass on flow surfaces influenced by the environment, we first need to understand how glass is distributed under baseline, air-quenched, conditions.

The modern Krafla flows are olivine tholeiitic basalts quenched solely by air, excluding ambient moisture from precipitation, or held in vegetation [7]. The flow field is adorned with low-sloped (<6°) elongated a'ā channels and broad central pāhoehoe fields, with discrete and transitionary roughness per the morphology [8]. The nature of olivine-glass presence, topography, and morphology makes Krafla attractive for comparative analysis to other basalt flows on Earth and to flows on Mars like Nili Patera, Syrtis Major Planum, which may contain a mixed olivine-glass signature [9].

On Krafla, we use VNIR satellite image data to constrain our methods for glass detection. We ground truth these data with *in-situ* handheld spectrometry to validate these spectra with total (average) reflectance and connect glass abundance to flow morphology.

Data and Methods: We use World-View 3 (WV3) spectral image data from 12 VNIR bands, 400 nm to 1040 nm, 1.24 m per pixel. WV3 data were radiometrically calibrated, atmospherically corrected, and orthocorrected before being pansharpened to 0.3 m per pixel. Bands >705 nm were contrast enhanced between images due to WV3 artifacts – likely a result from the low total reflectance of basalt. Raster values were then normalized to a global fit of the flow's delineated margin to highlight low reflectance maps. Handheld VNIR measurements use an ASD HALO spectrometer, 350 nm to 2500 nm, at ~2000 bands. Handheld measures were averaged 300 times per point.

Endmember Analysis: We use B5 + (B8/B7) to highlight Fe^{2+} absorptions near 900 and 1200 nm as our parameter for olivine and ferrous silicates [10]. We then use a normalized ratio (B3-B8)/(B3+B8) to differentiate between the similar absorption centers of olivine and glass at 1200 nm and to consider the lower total reflectance, or slope [11], of glass due to their ambiguous SiO_4 bond [5]. We validate the presence of olivine's split peak near 600 nm by compositing (B4).

Field Methods: Samples, field observations, aerial and ground photographs, and in-situ spectra were collected at each spectral endmember and morphology intersection [Fig. 1, 2]. Transects were made along the major northern channel, eastern outbreaks, and pāhoehoe-a'ā transitions. *In-situ* spectra are downsampled to WV3 bandwidths for comparison [Fig. 1].

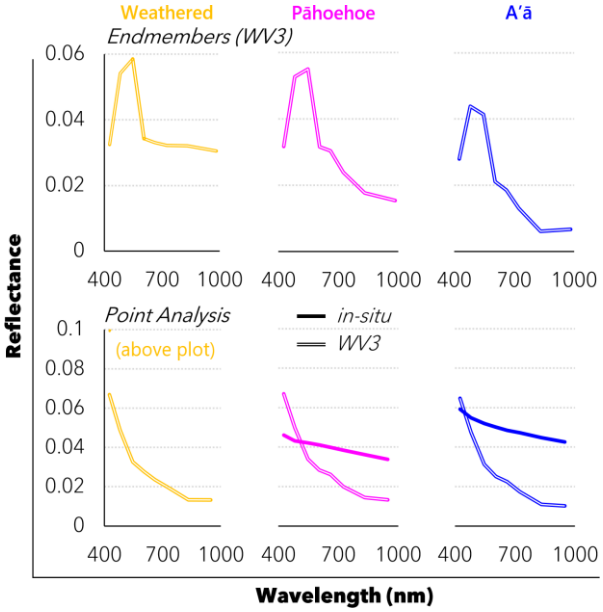

Figure 1: Spectral profiles of WV3 endmembers (top) and point analysis (bottom). Colors associate to the endmember morphology. Endmember spectra are shown as 100 averaged points within each unit.

Results and Discussion: Three diagnostic endmembers are found with differences in total (average) reflectance correlating to major flow morphologies [Fig. 1, 2]. Endmembers simplify to a'ā, pāhoehoe, and a grouping of oxidized unconsolidated material, lichen, and fumaroles. The order of total reflectance between endmembers changes from observations of satellite or *in-situ* data.

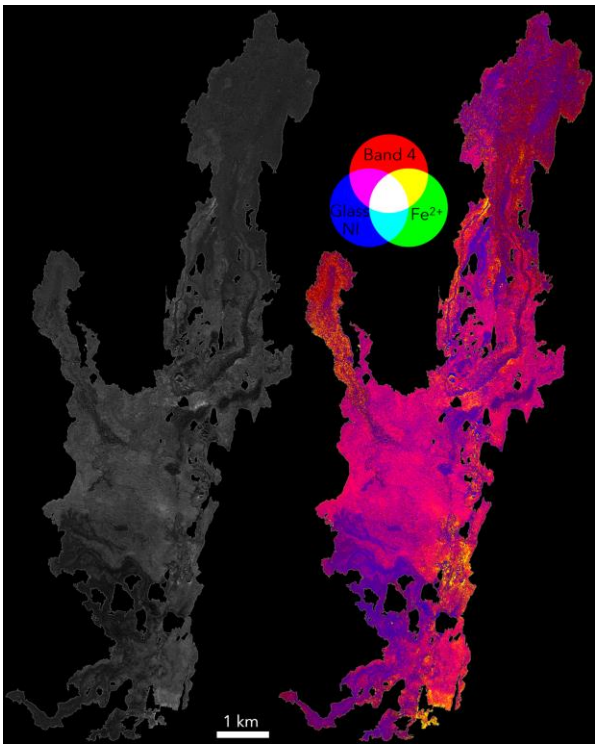

Figure 2: WV3 mosaics of delineated Krafla. Average visible spectra (left) and parameter composite (right).

The parameter map delineates Krafla's surface into diagnostic zones of smooth pāhoehoe intersected by a'ā channels feeding into smaller pāhoehoe or a'ā zones. On the parameter maps, total reflectance increases in order of a'ā, pāhoehoe, and organic or weathered materials. Presuming a consistent composition and roughness of each unit, there are 1 and 2σ variations in total reflectance that ignore morphological boundaries. When these areas are viewed from the parameter map, fine-scale flow features are revealed, such as slabby pāhoehoe, outbreaks, and margin interactions. Delineating these fine-scale features, the total reflectance then remains distinct from their parent morphology with similar spectral ratios.

In-situ measurements show an inverse order of total reflectance between pāhoehoe and a'ā. Pāhoehoe lobes show lower total reflectance than a'ā. The lowest *in-situ* total reflectance are smooth, central, inflated pāhoehoe lobes, breaches, and the flow margin. Near margins of the flow, we find areas of low reflectance are perturbed by higher reflectance exfoliation which may reveal interior, crystalline, basalt from weathering of the glassy crust. Interestingly, exfoliated samples show lower total reflectance on the original surface and higher total reflectance on the fresh surface.

In-situ measurements show a mismatched pattern of total reflectance with satellite data. Individual band analysis, in addition to total reflectance, may delineate glass most effectively from satellite data as opposed to either method alone. Point analysis of the lowest *in-situ* total reflectance pāhoehoe show negative slopes in WV3 band centers 832nm to 948nm while moderate a'ā show higher *in-situ* total reflectance and positive slopes in WV3 bands centers 832nm to 948nm.

Conclusion: We identified three endmembers in satellite VNIR imagery that provide guidance to areas where total reflectance is inconsistent with the surface morphology, suggesting differences may result from glass abundance. The creation of individual endmembers from the morphology-parameter combinations will be used for detailed inspection and future spectral unmixing of other quenched lava flow surfaces on Earth. Diffusion of light from surface roughness is problematic on a lava flow, and is difficult to calibrate on Earth due to atmospheric scattering and basalt's low reflectance [e.g., 12]. Because of these difficulties, creating an inventory of basaltic spectra with the introspection of total reflectance allows us to classify lava flows on Earth and Mars to detect glass and ancient areas of potential water-lava interaction. Where diffusion modeling is possible, like Mars or the Moon, the distribution of consolidated glass on lava flows may be applied in context to quenching agents with more accurate low-reflectance spectra.

References: [1] Wilson L. and Head J. W. (1994) *Rev. Geophys., 32, 221.* [2] Fagents S. A. et al. (2002) *London Geol. Soc.,* 295-317. [3] Reeder A. et al. (2019) *LPSC L,* 2132. [4] Glass B. P. (2016) *Int. J. Appl Glass Sci., 7,* 435-445. [5] Henderson M. J. B. et al. (2021) *Earth & Space Sci., 8, 2.* [6] Rader E. et al. (2021) *Icarus, 383, 115084.* [7] Rossi, M. (1997) *Geomorph., 1-2,* 95-112. [8] Aufaristama M. et al. (2016) *IOP Conf. Series: E&E Sci., 29, 012002.* [9] Fawdon P. et al. (2015) *JGR: Planets, 120, 5.* [10] Pour A. B. et al. (2019) *Remote Sens., 11, 20.* [11] Siebels K. et al. (2021) *Int. J. App. Earth Obs. Geoinfo., 96, 102259.* [12] Johnson J. R. and Grundy W. M. (2001) *GRL, 28, 10.*

Additional Information: This research is supported by the National Aeronautics and Space Administration Grant No. 80NSSC18K1518 and Grant No. 80NSSC21K1165. We thank the Icelandic Institute of Natural History and the Reykjahlioar Landowner Association for their permissions and Anna-Sage Browning, Alexandra Huff, Renee Jensen-Hasfurther, Sean Peters, and Tim Manus Photography for their field assistance.